31

Nuclear Cardiology: Its Role in the Detection and Management of Coronary Artery Disease

Richard M. Fleming

Nuclear imaging of the heart began with the discovery of x-rays emitted from uranium salts by Henry Becquerel in 1896. Radioactive materials were first used in 1926 when Herman Blumgart injected radon gas into arm veins and recorded the time necessary for the radioactivity to appear in the blood of the opposite arm.[1] This was known as the *circulation time,* which was prolonged in patients with heart disease. The first use of radioisotope scanning occurred in 1958 to detect pericardial effusion with a rectilinear scanning method.[2] The first attempt to detect myocardial infarction met with limited success because of too much tracer uptake in the stomach.[3] With the advent of the anger circuit,[4] the way was cleared for improved detection of cardiac abnormalities, particularly when coupled with technetium 99m imaging agents.

In the early 1970s[5] potassium 43 chloride was used to image the myocardium, and the search for more appropriate potassium analogs lead to the discovery of thallium 201 and rubidium 82. Despite popular misconceptions about thallium 201, this radionuclide follows regional blood flow as demonstrated in dogs.[6] Since then several additional isotopes[7–17] have been developed for use with planar and single photon emission computed tomography (SPECT) imaging of the heart. Additional investigation concerning the reversibility[7–10,18–32] of coronary atherosclerosis, using both SPECT and positron emission tomography (PET) imaging, has been possible in recent years with improvements in available isotopes and imaging techniques. This chapter focuses on the methods used to determine changes in coronary blood flow and the assessment of normal, ischemic, and infarcted myocardium using planar, SPECT, and PET imaging.

The Components of Nuclear Cardiac Imaging

There are several components to nuclear imaging of the heart that can lead to confusion when ordering and interpreting test results. The different types of tests available as well as their interpretation are discussed here. Before ordering a nuclear study, the physician must make three decisions. *First,* one must decide what type of camera (planar, SPECT, or PET) will best answer the question. *Second,* one must determine which form of stress will best bring out differences in blood flow between resting and physiologically stressed conditions. Of course, this is not a consideration when ordering a resting ventriculogram (RVG), which has other names including multiple gated analysis (MUGA). (*Gated* means that images are matched with electrocardiogram activity to differentiate systole from diastole.) The MUGA can be either a resting or stressed (usually bicycle) study used to determine the ejection fraction of either the right (first-pass) side of the heart or the left ventricle. These studies can also be used to determine if there are shunts (atrioseptal defect, ventriculoseptal defect, patent ductus arteriosus, etc.), regurgitant valves (mitral, etc.), or regional wall motion abnormalities (Figure 31.1) such as would be seen with atherosclerotic heart disease. *Finally,* a decision must be made about the type of radionuclide to be used. Radionuclides are the radioactive compounds injected into the patient and subsequently detected by the camera. These radioactive materials are not called *radionucleotides* (radioactively labeled nucleic acids), but *radionuclides.*

For the purpose of this chapter we do not further address RVG/MUGA studies. Instead we focus our attention on planar, SPECT, and PET imaging of the heart, allowing us to develop a better understanding of these tests.

Types of Cameras

There are currently three major types of cameras available for cardiac imaging. These include planar, SPECT, and PET cameras. Each uses photomultiplier tubes

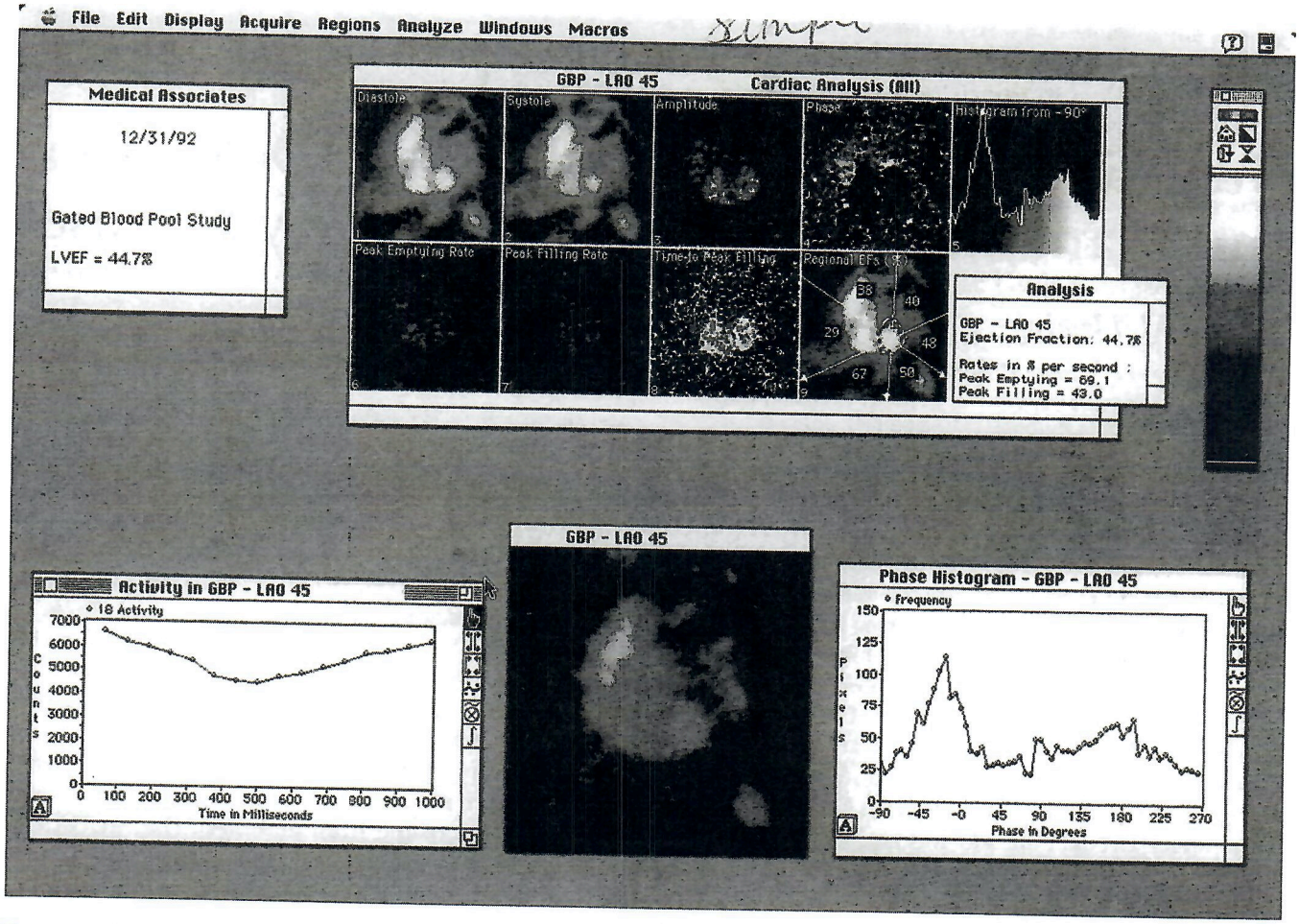

FIGURE 31.1. Gated blood pool imaging. Regional wall motion abnormalities, first-pass (right ventricle ejection fraction) and multiple-gated analysis of the left ventricle was assessed using 1 mCi of "cold" pyrophosphate and 26 mCi of technitium 99m. Initial imaging of the right ventricle demonstrated a right ventricle ejection fraction of 22% (not shown here). Imaging of the left ventricle is statically displayed here showing the diastolic and systolic activity and histogram curves that are used to assess left ventricle ejection fraction, which was 44.7%. The images represented here were obtained from the left anterior oblique position and are divided into specific regions (regional ejection fractions) as shown in the last square of the top two rows of images. These regional ejection fractions demonstrate mildly depressed ejection fractions anteriorly, consistent with left anterior artery disease.

(PMTs) designed to absorb different levels of energy (photons) and convert them into electrical signals interpreted by the computer as radioactivity. Planar and SPECT cameras also utilize crystals and collimators designed to reduce extraneous information and improve their accuracy. The radioactivity being detected by the cameras presumably comes from the patient who has been injected with an appropriate radioactive compound. However, neither planar nor SPECT imaging has a mechanism to totally exclude other sources of radiation from being interpreted by the computer as coming from the patient. The primary difference between planar and SPECT imaging is that in SPECT imaging, the camera moves around the patient, whereas the camera operator must position the camera for planar imaging.

Figure 31.2 shows how radioactivity from outside the patient could be recognized by the camera as coming from the patient and how radioactivity coming from the patient may not be detected but may be absorbed or sufficiently diminished by the time it reaches the collimators. The energy released by radioisotopes that can be

TABLE 31.1. Planar and single photon emission computed tomography isotopes.

Isotope	Radionuclide	Physical half-life (h)	Imaging energy
Thallium 201	Ti 201	73	67–82 KeV
Teboroxime	Tc 99m	6	140 KeV
Sestamibi	Tc 99m	6	140 KeV

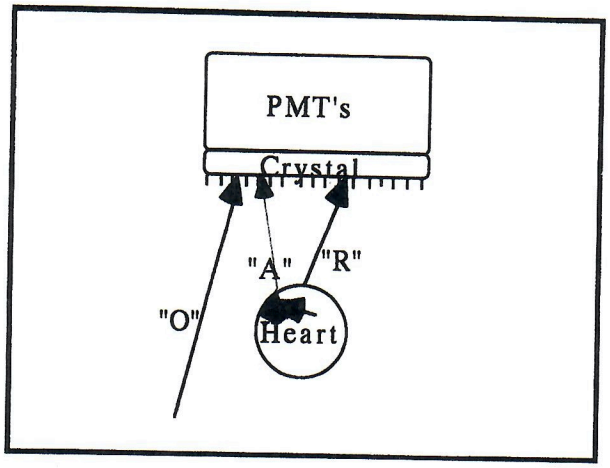

FIGURE 31.2. Planar and SPECT imaging. Radioactivity (R) passes through the collimator and is then detected by the scintillation crystal, after which it is converted to electrical information by photomultiplier tubes (PMTs). The computer records these events as coming from the patient following the injection of radioactive isotopes. Other sources of radioactivity may be interpreted as coming from the patient (O) when in fact they are not. Similarly, activity coming from the patient (A) may not be detected because of energy loss en route to the SPECT camera.

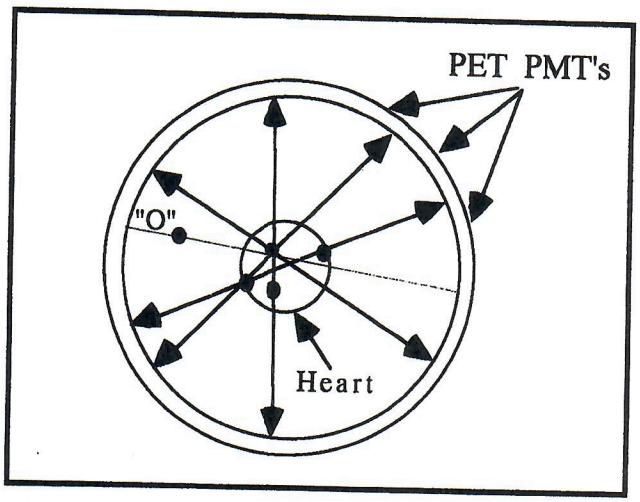

FIGURE 31.3. PET imaging. Patients are placed within circular rings of PMTs that detect positron–electron annihilation events (filled circles) and record these events as coming only from the patient. Those events originating outside the region of the heart (O) are excluded. Attenuation is corrected for by gallium scanning earlier in the study. See text for full details.

best detected by planar and SPECT systems ranges from 60 to 180 keV. This means that technetium compounds (Table 31.1), which have a photon energy of 140 keV are ideal for SPECT imaging.

Unlike planar and SPECT systems, the PET camera is designed to detect two different photons released simultaneously when a positron (antimatter electron) from a PET isotope (Table 31.2) injected into the patient collides with an electron from the patient. When this happens, the mass of the positron and the mass of the electron are converted into two photons of energy ($E = mc^2$), each having 511 keV and traveling in essentially opposite directions (Figure 31.3). These photons are almost simultaneously detected by two opposing PMTs. Because photons travel at the speed of light, the time necessary for both photons to reach PMTs on opposite sides of the patient can be calculated by knowing how far the heart is from the PMTs. Using this information (time-of-flight) virtually eliminates errors in determining the source of radioactivity, which increases the sensitivity and specificity of PET imaging as compared with either SPECT or planar methods.

TABLE 31.2. Position emission tomography isotopes.

Isotope	Source	Physical half-life (h)	Imaging energy
18-Fluoro-2-deoxyglucose	Cyclotron	110 min	511 keV
Ammonia 13	Cyclotron	10 min	511 keV
Rubidium 82	Generator	75 s	511 keV

Types of Physiologic Stress

Many clinicians still consider there to be only one method for inducing changes in coronary artery blood flow; such changes are frequently referred to as *stressing the heart.* In reality there are two major approaches available. The first is to increase the heart rate and blood pressure by walking on a treadmill or bicycling, thereby increasing the heart's demand for blood, as described in Chapter 29 on atherosclerosis. Using well-established protocols, the intensity of the exercise is gradually increased until one of several things happen. These events include but are not limited to reaching at least 85% of the patient's maximal predicted heart rate (determined by age [Table 31.3]); developing a hypertensive response to exercise (e.g., diastolic blood pressure greater than 100 to 110 mm Hg); cerebrovascular accident; developing a potentially fatal dysrhythmia; developing angina; ischemia or infarction as demonstrated on the electrocardiogram, regardless of symptoms; exertional dyspnea; hypotensive response to exercise (indicative of left ventricular dysfunction); leg fatigue; or physical exhaustion. In all but the first of these scenarios (reaching 85% of the maximal predicted heart rate), the patient does not attain the necessary hemodynamic response required to produce sufficient changes in coronary blood flow to detect differences between the stressed and resting states.

Alternatively, pharmacologic approaches have been developed[7–10] to cause sufficient changes in blood pressure and heart rate to elicit a meaningful stress response in patients, while minimizing potential problems and side effects. A comparison of the expected hemody-

TABLE 31.3. Maximum predicted heart rate by age.

Age	20	25	30	35	40	45	50	55	60	65	70	75	80	85
Heart rate	197	195	193	191	189	187	184	182	180	178	176	174	172	170

TABLE 31.4. Hemodynamic results of different stressors.*

	Percent change in heart rate	Percent change in systolic pressure	Percent change in diastolic pressure
Dipyridamole	45.5 ± 22.2	−8.3 ± 11.3	−9.6 ± 8.0
Dobutamine	77.0 ± 28.8	19.4 ± 31.4	−8.9 ± 14.3
Treadmill	89.5 ± 35.1	31.3 ± 18.5	4.22 ± 11.3

*Values are displayed as mean plus or minus standard deviation.

namic results as well as the possible side effects for both dobutamine and high-dose dipyridamole (HDD) are listed in Tables 31.4 and 31.5, respectively. The protocols for using these agents are shown in Figures 31.4 and 31.5, which also include the approach used with exercise (treadmill) testing, in addition to minor differences in timing needed for each of the available isotopes used with planar, SPECT, and PET imaging. Patients should not receive dipyridamole if there is any evidence of pulmonary disease or allergies to the drug. Full details of these approaches are discussed elsewhere.[7]

Because differences in blood flow between resting and stressed states should be maximized, the clinician must carefully choose the approach to be used, otherwise the study will provide little or no useful information. The cost and risks to the patient in these circumstances cannot be totally justified if meaningful results are not obtained. The results of exercise (treadmill) testing and SPECT imaging are usually reported together. Discrepancies between the treadmill tests and nuclear imaging results are well known[9,10] and should be considered in light of the limitations of each method.

PET imaging protocols have an added component that is used to improve the accuracy of the information obtained as compared with SPECT and planar imaging. This is seen in protocol A of Figure 31.5, which shows the various PET protocols used for assessing coronary artery blood flow and myocardial viability. This additional component (attenuation correction) determines the effect of tissue energy loss (attenuation) and corrects for diminished photon energy reaching the PMTs as a result of the effect of individual patient body mass and air surrounding the patient. Planar and SPECT imaging may have artifacts from both diaphragmatic (inferior wall of heart) and breast (anterior wall) attenuation, resulting in false positive results.

To determine the PET attenuation correction, a Plexiglas ring is placed around the patient; 3 mCi of gallium 68 is administered, and counts are collected until 200 million counts are recorded. This information is used by the computer to determine how much energy attenuation is occurring, thereby improving the accuracy of the detection of attenuated photons from different regions of the heart (as detected by each PMT surrounding the patient). The full procedure for PET imaging is shown in Figure 31.5.

TABLE 31.5. Percentage of patients reporting side effects with pharmacological stress.

	Dipyridamole	Dobutamine
Chest pressure	41.3	20.0
ST-segment depression	25.3	20.0
Headache	9.3	0.0
Nonspecific ST changes	6.7	0.0
Nausea	6.7	0.0
Dyspnea	5.3	0.0
Increased ventricular ectopy	4.0	40.0
Flush	2.7	0.0

Radionuclides (Tracers)

There are numerous radionuclides currently available, and their use depends on the clinical question being asked and the type of camera system being employed. The radionuclides are used in conjunction with a specific stress protocol (Figures 31.4 and 31.5) to obtain resting and stress images. Interestingly, when PET is employed, the rest image is obtained first, giving useful information regarding any prior myocardial infarction, whereas planar and SPECT protocols almost always begin with the stress component, which has the potential to precipitate problems in the absence of baseline information. At our institute, we perform all nuclear cardiac studies using the rest/stress approach.

The availability of 18-fluoro-2-deoxyglucose (FDG) has made it possible to determine myocardial viability when given to patients who are not fasting. When a fasting state exits, the results are uninterpretable because the heart obtains its energy from the metabolism of fatty acids while suppressing the metabolism of glucose. For FDG to be useful, the patient must be in a nonfasting state so that glucose will be taken up by myocardial cells and used for cellular metabolism. This is why patients (who must be

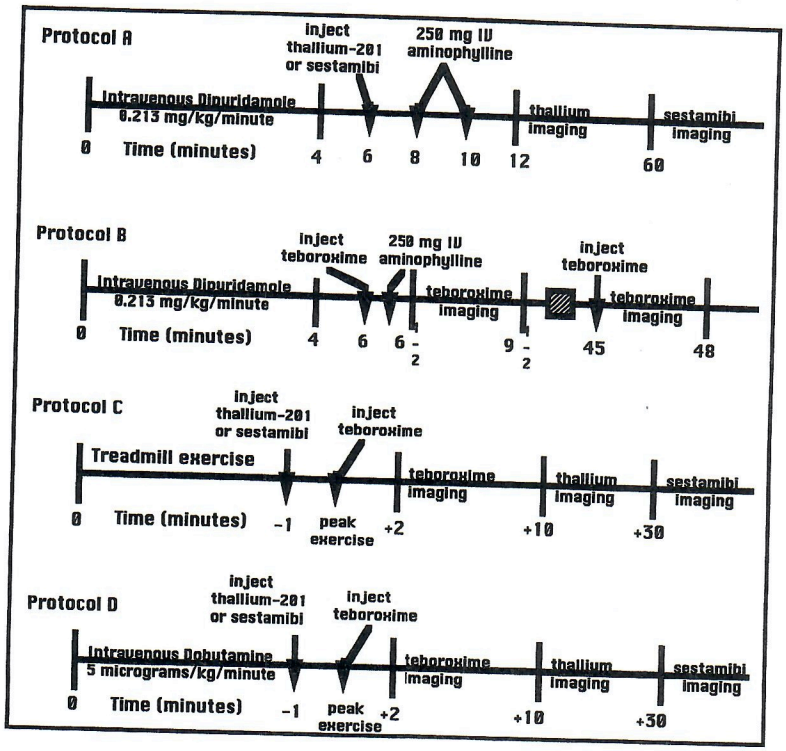

FIGURE 31.4. Stress protocols used for planar and SPECT imaging. Protocols A and B utilize high-dose dipyridamole (HDD) for the radionuclides thallium, Tc 99m hexakis-2-methoxy-2-isobutyl isonitrile (sestamibi), and Tc 99m chloromethyl-boron(1-)-tris[1,2-cyclohexane-dionedioxime(1)] (teboroxime). Protocols C and D are used for exercise treadmill testing and intravenous dobutamine, respectively.

fasting for protocols B and C) are given 50 grams of glucose at the beginning of protocol D. Since FDG can be taken up by both viable and ischemic myocardium, blood flow must also be determined with ammonia-13 to determine if the region has normal or ischemic blood flow. After a myocardial infarction, a region of the heart occluded from the blood supply shifts to the anaerobic metabolism of glucose, leading to intense uptake of glucose in that region. Additional FDG activity in this region may be related to phagocytosis of myocardial cellular debris by white blood cells. It is probably for these reasons that patients who have recently undergone a myocardial in-

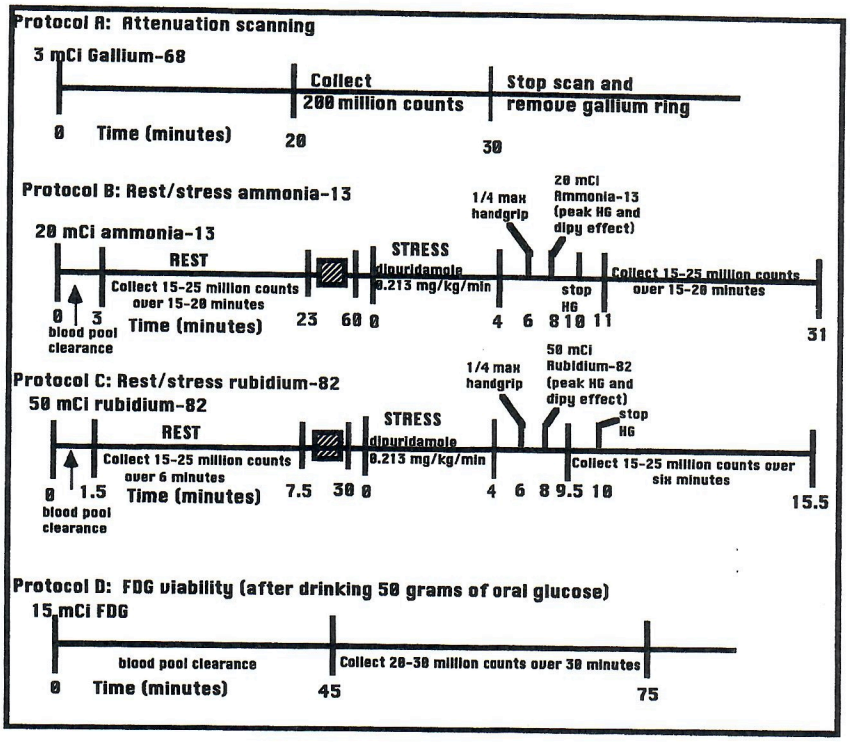

FIGURE 31.5. PET imaging protocols for determining attenuation correction, coronary blood flow, and myocardial viability. Protocol A illustrates the procedure for attenuation correction, which must be done before protocol B, C, or D. Protocols B and C display the procedure used for assessing coronary artery blood flow using ammonia 13 and rubidium 82. The hand grip needed to increase sympathetic nervous system activity is determined by having the patient demonstrate maximum grip strength prior to the study. The patient is then asked to exhibit a grip strength (measured) of one-quarter maximum during the stress component of the study to augment the dipyridamole effect. Protocol D demonstrates the procedure for assessing myocardial viability using 18-fluoro-2-deoxyglucose (FDG). See text for full details.

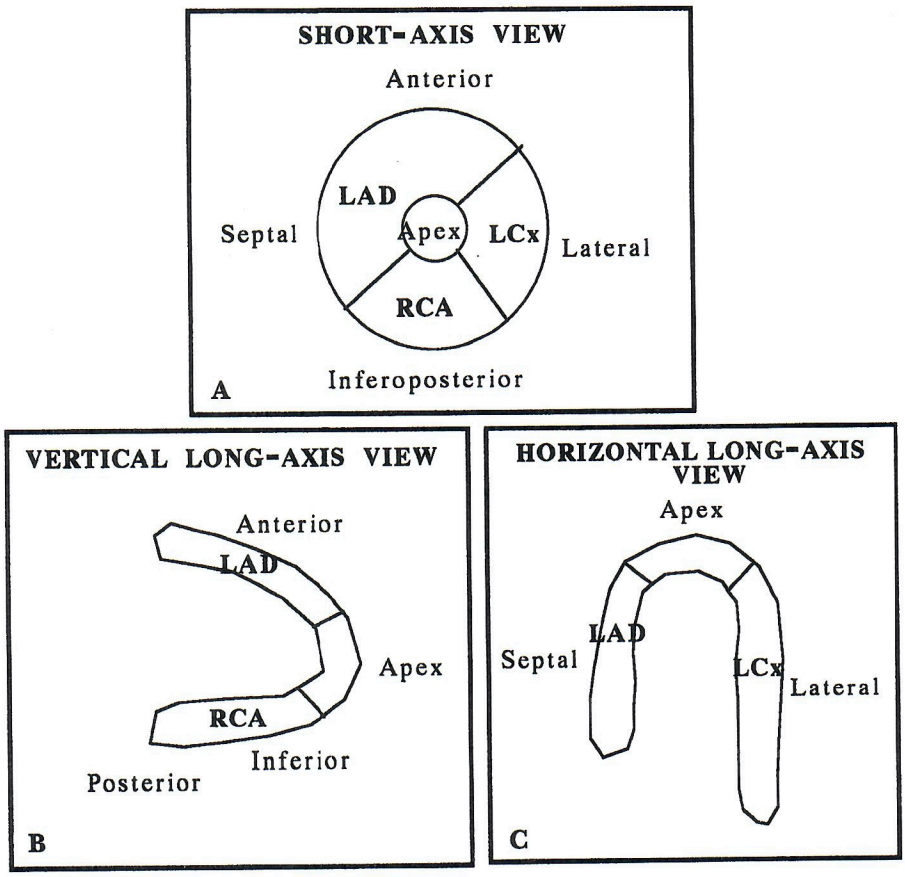

FIGURE 31.6. Relative regions of myocardial blood flow in relationship to reconstructed images from nuclear imaging. **A** represents a reconstructed short-axis view of the heart showing the anterior, septal, apical, inferoposterior, and lateral walls. This same presentation is used for bull's-eye displayed images. **B** represents a reconstructed vertical long-axis view along with the locations of the anterior, apical, inferior, and posterior regions. Likewise, **C** shows the septal, apical, and lateral walls of the heart as represented on the horizontal long-axis view. The correlating arterial distributions are shown as RCA (right coronary), LAD (left anterior descending), and LCx (left circumflex) arteries. The apex is frequently supplied by the LAD, but this may vary depending on the coronary anatomy of the patient.

farction may demonstrate a false positive uptake of FDG when the tissue is in fact necrotic.

Diabetic individuals may also give unpredictable FDG uptake patterns, whether they have taken their usual dose of insulin or not, suggesting that they have nonviable tissue because of failure to take up glucose (FDG) even though the myocardium has normal perfusion and function.

Review of images using planar, SPECT, and PET approaches is accomplished via computer reconstructions that are displayed as short-axis, vertical long-axis, and horizontal long-axis views. Diagrams of these three different views are shown in Figure 31.6, along with the most common arterial distribution found in each specific region. Regions of the myocardium are then compared for the amount of tracer activity present, which is defined as normal, reduced, or absent. These ratings are subjective and vary depending[8] on reader interpretation and experience. Once the rest and stress images are interpreted individually, they are compared to determine if the different regions of myocardium are normal, ischemic, or infarcted, as shown in Table 31.6. Based on the experience and training of the individual and the type of camera (planar, SPECT, or PET) used, the sensi-

TABLE 31.6. Interpretation of nuclear cardiac imaging.

Planar and single photon emission computed tomography image interpretation			
Resting image	Stress image	Interpretation	
Normal	Normal	Normal	
Normal	Decreased or absent	Ischemia	
Decreased or absent	Decreased or absent	Infarcted	
Positron emission tomography image interpretation			
Resting image	Stress image	FDG* result	Interpretation
Normal	Normal	Normal	Normal and viable
Normal	Decreased or absent	Normal	Ischemic but viable
Normal	Decreased or absent	Decreased or absent	Ischemic and necrotic
Decreased or absent	Decreased or absent	Decreased or absent	No flow and necrotic

FDG, 18-fluoro-2-deoxyglucose.

TABLE 31.7. Sensitivity and specificity of nuclear imaging techniques.

	Percent sensitivity	Percent specificity
Planar	60–70	50–60
Single photon emission computed tomography	70–90	60–80
Positron emission tomography	92–96	92–100

tivity and specificity of the results can vary widely, as shown in Table 31.7. Recently, it has been shown that PET is not only more cost-effective in the detection of coronary artery disease,[33] but results in greater extension of quality-adjusted life years as a result of treatment based on the test results. However, with the use of HDD protocols and attenuation correction of SPECT imaging, SPECT results are approaching that of PET.

Interpretation of test results must be considered as a physiologic parameter of atherosclerosis, as described in Chapter 29. Reductions in stenosis flow reserve as detectable by nuclear imaging may not be well appreciated on coronary arteriography[34–36] because of coronary angiography's inherent limitations in the detection of anatomic changes. When PET was compared with coronary arteriography,[33] individuals with less than 70% pretest probability of coronary artery disease demonstrated a lower cost per effect with PET than with coronary arteriography and both SPECT and PET can detect "early" CAD that angiograms can miss.

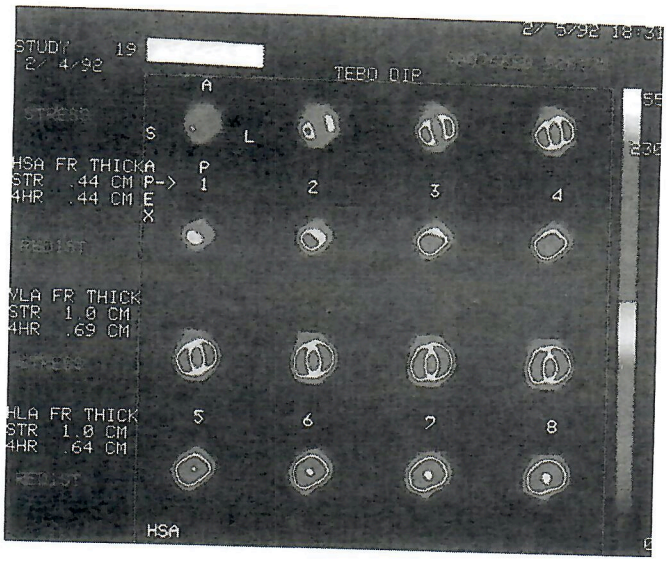

FIGURE 31.7. Example of SPECT imaging. Reconstructed short-axis images are seen in rows 1 through 4. Rows 1 and 3 reveal stress images, whereas rows 2 and 4 show rest images of the same regions. Images are compared using the qualitative scale to the right of the images, ranging from the highest blood flow (top) to the least (bottom). This study demonstrates ischemia in the anterior and inferior regions of the heart, consistent with coronary artery disease. See text for full details.

Examples of Nuclear Cardiac Perfusion Studies

A comparison of resting coronary artery blood flow is made with maximally obtainable (stress) blood flow, regardless of camera type, form of radionuclide, or type of stress used to induce changes in coronary blood flow. The reconstructed images are compared (Table 31.6) and results reported for each region of the myocardium. The regions are designed to yield useful information regarding the blood flow in each coronary artery (Figure 31.6).

Figure 31.7 shows the results of a patient who underwent stress imaging with dipyridamole using a technetium 99m compound. The images shown represent short-axis (coronal) images that have been reconstructed by the computer. Rows 1 (top) and 3 (second from the bottom) display the relative tracer activity during dipyridamole-induced stress. Rows 2 (second from the top) and 4 (bottom) show the same regions of myocardium during the resting component of the study. Each image (slice) shows the anterior (A), lateral (L), inferoposterior (P), and septal (S) walls. To the right of the images is a gray scale ranging from highest flow (greatest isotope activity, top) to the least amount of activity (bottom). The central part of most of the images is blue-green, which represents the left ventricular chamber where there are no coronary arteries.

Image slices 1 through 8 represent matched stress and rest images beginning at the apex of the heart and proceeding upward to the base of the heart. Stress images in rows 1 and 3 demonstrate less tracer activity in the anterior (A) and inferoposterior (P) distributions of the heart. This same patient had a 64% narrowing of the proximal left anterior descending artery (A), a 72% narrowing of the right coronary artery (P), and a 26% narrowing of the left circumflex artery (L), as measured by quantitative coronary arteriography as described in Chapter 29 on atherosclerosis. The resting images reveal normal blood flow. These findings of normal blood flow at rest and decreased blood flow under stress represent ischemia in the right coronary and left anterior descending coronary arteries.

Figure 31.8 shows the results of a patient who underwent dipyridamole PET imaging using ammonia 13 and FDG to determine myocardial blood flow and viability, respectively. Assessment of myocardial blood flow was performed using the protocols shown in Figure 31.5, with reconstructed images displayed using bull's-eye equivalent images as explained in Figure 31.6. Images are compared using the qualitative scale at the bottom of the reconstructed images: the right represents the highest blood flow and the left the least. The stress image is displayed on the left of Figure 31.8; the corresponding rest image is displayed in the center. Intensity

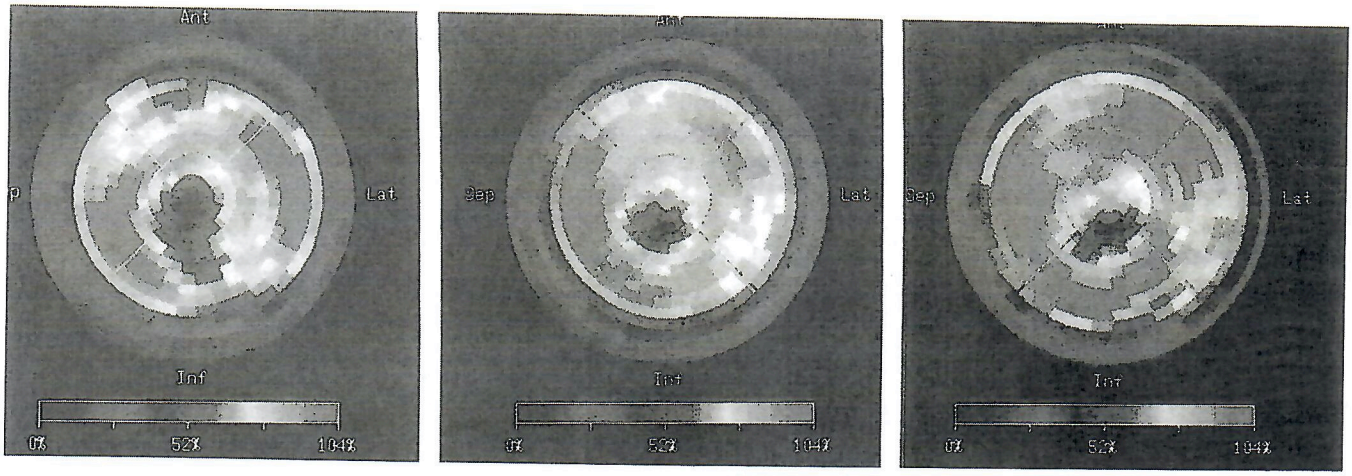

FIGURE 31.8. Example of PET perfusion imaging using ammonia 13. Images are presented using a bull's-eye equivalent approach, with the apex at the center of each image, the anterior wall at 12 o'clock, the lateral wall at 3 o'clock, the inferior wall at 6 o'clock, and the septum at 9 o'clock. The tracer activity is depicted using the qualitative scale at the bottom, where the greatest activity is represented on the right and the least on the left. The first image (left) shows the result after injection of 20 mCi of ammonia 13 following high-dose dipyridamole and handgrip-induced stress. The center image represents the corresponding resting image after 20 mCi are injected at rest. The stress image shows decreased tracer activity in the anterior, apical, and inferior walls of the heart when compared with the resting image. See text for full details. Assessment of myocardial viability using FDG (right) was performed at rest after the ingestion of 50 grams of oral glucose and 15 mCi of FDG. Image acquisition began 45 min after injection with FDG, providing adequate time for blood pool clearance of FDG. Normal tracer activity is detected in all but the apical distribution of the myocardium, indicating that the apex is necrotic and the remainder of the myocardium is viable. See text for full details.

Image Number _____ Reader Number 0 1 2 3 4 5 6

Please circle the reader ID# and record the image # above.
Please circle the appropriate myocardial perfusion image (MPI) result for each region.

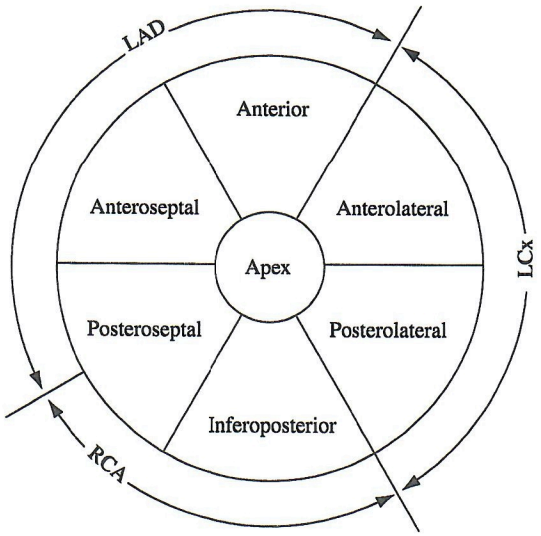

LAD = Left Anterior Descending Artery
LCx = Left Circumflex Artery
RCA = Right Coronary Artery

	Myocardial perfusion rating*					
Anterior	0	1	2	3	4	5
Anteroseptal	0	1	2	3	4	5
Posteroseptal	0	1	2	3	4	5
Inferoposterior	0	1	2	3	4	5
Posterolateral	0	1	2	3	4	5
Anterolateral	0	1	2	3	4	5
Apex	0	1	2	3	4	5

* 5 = normal, 4 = probaby normal, 3 = mild defect,
2 = moderate defect, 1 = severe defect, 0 = no perfusion

REST

the Center for Clinical Cardiology & Research

FIGURE 31.9. Protocols used at the Fleming Heart & Health Institute for qualitative reporting of myocardial perfusion imaging or myocardial viability. Each image (rest, stress, and viability) is evaluated to determine tracer activity in each of seven regions of the myocardium. These regions correlate to each of the three major (LAD, LCx, and RCA) epicardial arteries. Tracer activity is reported on a continuum from no perfusion (0) to normal perfusion (5).

of tracer activity (representing coronary blood flow) is decreased in the inferoposterior and apical regions during the stress component of the study, but improves during the rest imaging. This is consistent with ischemia in this region of the myocardium but does not define whether the heart is viable or infarcted.

The far-right image in Figure 31.8 represents myocardial viability assessment using FDG in the same patient. All images occurred at rest using the same approach to reconstruct images as previously discussed. The inferoposterior regions demonstrate normal FDG uptake, indicating ischemic but viable (Table 31.6) myocardium. In contrast, the apical region does not metabolize FDG and represents ischemic or infarcted myocardium.

Conclusion

The role of nuclear cardiology is continuing to expand as needs for improved, noninvasive assessment of coronary artery disease increase. The ability to qualitatively (Figure 31.9) determine myocardial perfusion imaging and myocardial viability with PET and SPECT[37-41] provides physiologic information that coronary arteriography cannot provide. Recent improvements in available isotopes, better and safer approaches to physiologically stress the heart, and improvements in both SPECT and PET imaging have increased the utility and diagnostic accuracy of these tests. The ability to detect subtle changes in stenosis flow reserve before changes in percent diameter stenosis can be detected on coronary arteriography (see Chapter 29) has resulted in many physicians recognizing an increased need and role for nuclear cardiac imaging using either SPECT or PET technologies. Additionally, myocardial perfusion imaging (MPI) also allows the physician to determine if angioplasty or bypass surgery will benefit myocardium which is supplied by a stenosis artery.

References

1. Blumgart HL, Weiss S. Studies on the velocity of blood flow, III: the velocity of blood flow and its relation to other aspects of the circulation in patients with rheumatic and syphilitic heart disease. *J Clinic Invest.* 1927;4:149–171.
2. Rejali AM, MacIntyre WJ, Friedell HL. A radioisotopic method of visualization of blood pools. *Am J Roentgenol.* 1958;79:129–137.
3. Dreyfuss F, Ben-Porath M, Menczel J. Radioiodine uptake in the infarcted heart. *Am J Cardiol.* 1960;6:237–245.
4. Anger HO. Scintillation camera. *Rev Sci Instrum.* 1958; 29:27.
5. Hurley PJ, Cooper M, Reba RC, et al. Potassium-43: a new radiopharmaceutical for imaging the heart. *J Nucl Med.* 1971;12:516–519.
6. Forman R, Kirk ES: Thallium-201 accumulation during reperfusion of ischemic myocardium: dependence on regional blood flow rather than viability. *Am J Cardiol.* 1984; 54:659–663.
7. Fleming RM, Rose CH, Feldmann KM: Comparing a high-dose dipyridamole SPECT imaging protocol with dobutamine and exercise stress testing protocols. *Angiology.* 1995; 46:547–556.
8. Fleming RM, Kirkeeide RL, Taegtmeyer H, et al. Comparison of technetium-99m teboroxime tomography with automated quantitative coronary arteriography and thallium-201 tomographic imaging. *J Am Coll Cardiol.* 1991;17: 1297–1302.
9. Fleming RM, Gibbs HR, Swafford J. Using quantitative coronary arteriography to redefine SPECT sensitivity and specificity. *Am J Physiol Imaging.* 1992;7:59–65.
10. Fleming RM. Detecting coronary artery disease using SPECT imaging: a comparison of thallium-201 and teboroxime. *Am J Physiol Imaging.* 1992;7:20–23.
11. Seldin DW, Johnson LL, Blood DK, et al. Myocardial perfusion imaging with technetium-99m SQ 30217: comparison with thallium-201 and coronary anatomy. *J Nucl Med.* 1989;30:312–319.
12. Hendel RC, McSherry B, Karimeddini M, et al. Diagnostic value of a new myocardial perfusion agent, teboroxime (SQ 30,217), utilizing a rapid planar imaging protocol: preliminary results. *J Am Coll Cardiol.* 1990;16:855–861.
13. Iskandrian AS, Heo J, Nguyen T, et al. Myocardial imaging with Tc-99m teboroxime: technique and initial results. *Am Heart J.* 1991;121:889–894.
14. Iskandrian AS, Heo J, Kong B, et al. Use of technetium-99m isonitrile (RP-30A) in assessing left ventricular perfusion and function at rest and during exercise in coronary artery disease, and comparison with coronary arteriography and exercise thallium-201 SPECT imaging. *Am J Cardiol.* 1989;64:270–275.
15. Sinusas AJ, Beller GA, Smith WH, et al. Quantitative planar imaging with technetium-99m methoxyisobutyl isonitrile: comparison of uptake patterns with thallium-201. *J Nucl Med.* 1989;30:1456–1463.
16. Gibbons RJ, Verani MS, Behrenbeck T, et al. Feasibility of tomographic technetium-99m-hexakis-2-methoxy-2-methylpropyl-isonitrile imaging for the assessment of myocardial area at risk and the effect of acute treatment in myocardial infarction. *Circulation.* 1989;80:1277–1286.
17. Trobaugh GB, Wackers FJTh, Sokole EB, et al. Thallium-201 myocardial imaging: an interinstitutional study of observer variability. *J Nucl Med.* 1978;19:359–363.
18. Ornish D, Brown SE, Scherwitz L, et al: Can lifestyle changes reverse coronary heart disease? *Lancet.* 1990;336: 129–133.
19. Fleming RM, Ketchum K, Fleming DM, et al. Treating hyperlipidemia in the elderly. *Angiology.* 1995;46:1075–1083.
20. Fleming RM., Ketchum K, Fleming DM, et al. Assessing the independent effect of dietary and hypolipemic medications on serum lipids. *Angiology.* 1996;47:831–840.
21. Fleming RM. *How to Bypass Your Bypass: What Your Doctor Doesn't Tell You About Cholesterol and Your Diet.* Bethel, Conn: Rutledge Books; 1997.
22. Fleming RM, Rater D, Ketchum K. Reducing cholesterol and triglycerides in the elderly patient by diet alone. Paper presented at: Council on Arteriosclerosis for the 66th Scientific Sessions of the AHA; November 8–11, 1993; Atlanta, Ga.

23. Fleming RM, Rater D. Dietary changes without medication can equally reduce cholesterol in both the young and older patient. Paper presented at: Council on Arteriosclerosis for the 66th Scientific Sessions of the AHA; November 8–11, 1993; Atlanta, Ga.
24. Fleming RM, Rater D, Ketchum K. Studying the effect of medications on cholesterol and triglycerides in subjects not receiving dietary counseling. Paper presented at: Council on Arteriosclerosis for the 66th Scientific Sessions of the AHA; November 8–11, 1993; Atlanta, Ga.
25. Fleming RM, Ketchum K. Dietary reinforcement is an integral component of cholesterol reduction. Paper presented at: Council on Arteriosclerosis for the 66th Scientific Sessions of the AHA; November 8–11, 1993; Atlanta, Ga.
26. Fleming RM, Fleming DM, Gaede R. Hyperlipidemic elderly patients: comparing diet and drug therapy. Paper presented at: Council on Arteriosclerosis for the 67th Scientific Sessions of the AHA; November 14–17, 1994; Dallas, Tex.
27. Fleming RM, Fleming DM, Gaede R. Treatment of hyperlipidemic patients: diet versus rug therapy. Paper presented at: Council on Arteriosclerosis for the 67th Scientific Sessions of the AHA; November 14–17, 1994; Dallas, Tex.
28. Fleming RM. Comparing the results of SPECT imaging using high-dose dipyridamole, dobutamine and treadmill stress. Paper presented at: Council on Arteriosclerosis for the 67th Scientific Sessions of the AHA; November 14–17, 1994; Dallas, Tex.
29. Fleming RM. Arteriosclerosis as defined by quantitative coronary arteriography. Paper presented at: Council on Arteriosclerosis for the 67th Scientific Sessions of the AHA; November 14–17, 1994; Dallas, Tex.
30. Fleming RM, Ketchum K, Fleming D, et al. Controlling hypercholesterolemia by diet and drug therapy in the elderly. First Annual Scientific Session on Cardiovascular Disease in the Elderly; March 18, 1995; New Orleans, La.
31. Fleming RM. Reducing cholesterol and triglyceride levels in both the young and elderly patient, by dietary changes: with and without hyperlipidemic medications. 17th World Congress of the International Union of Angiology; April 3–7, 1995; Westminister, London.
32. Fleming RM, Ketchum K, Fleming DM, et al. Investigating differences in cholesterol and triglyceride levels as influenced by diet and hyperlipidemic medications. 42nd Annual World Assembly of the American College of Angiology; October 15–20, 1995; Maui, Hawaii.
33. Patterson RE, Eisner RL, Horowitz SF. Comparison of cost-effectiveness and utility of exercise ECG, single photon emission computed tomography, positron emission tomography, and coronary arteriography for diagnosis of coronary artery disease. *Circulation.* 1995;91:54–65.
34. Fleming RM, Kirkeeide RL, Smalling RW, et al. Patterns in visual interpretation of coronary arteriograms as detected by quantitative coronary arteriography. *J Am Coll Cardiol.* 1991;18:945–951.
35. Fleming RM, Fleming DM, Gaede R. Training physicians and health care providers to accurately read coronary arteriograms: a training program. *Angiology.* 1996;47:349–359.
36. Fleming RM, Harrington GM. Quantitative coronary arteriography and its assessment of atherosclerosis, II: calculating stenosis flow reserve from percent diameter stenosis. *Angiology.* 1994;45:835–840.
37. Reske SN, Knapp FF, Winkler C. Experimental basis of metabolic imaging of the myocardium with radioiodinated aromatic free fatty acids. *Am J Physiol Imaging.* 1986; 1:214–229.
38. Fleming RM, Feldmann KM, Fleming DM. Comparing a high dose dipyridamole SPECT imaging protocol with dobutamine and exercise stress testing protocols, II: using high-dose dipyridamole to determine lung-to-heart ratio. *Int J Angiol.* 1988;7:325–328.
39. Fleming RM, Feldmann KM, Fleming DM. Comparing a high-dose dipyridamole SPECT imaging protocol with dobutamine and exercise stress testing protocols, III: using dobutamine to determine lung-to-heart ratios, left ventricular dysfunction, and a potential viability marker. *Int J Angiol.* 1999;8:22–26.
40. Fleming RM. The clinical importance of risk factor modification: looking at both myocardial viability (MV) and myocardial perfusion imaging (MPI). *Int J Angiol.* Submitted.
41. Fleming RM. The importance of physiologic information from cardiac PET in assessing coronary artery disease in people with "normal" coronary angiograms. *Int J Angiol.* Submitted.